Linear analysis and crossphase dynamics in the CTEM fluid model

Physics of Plasmas

RESEARCH ARTICLE | FEBRUARY 09 2024

Linear analysis and crossphase dynamics in the CTEM fluid model FREE

M. Leconte ; Lei Qi ; J. Anderson

Phys. Plasmas 31, 022302 (2024)
https://doi.org/10.1063/5.0179680

Linear analysis and crossphase dynamics in the CTEM fluid model

Cite as: Phys. Plasmas **31**, 022302 (2024); doi: 10.1063/5.0179680
Submitted: 4 October 2023 · Accepted: 7 January 2024 ·
Published Online: 9 February 2024

M. Leconte,[1,a)] Lei Qi,[1] and J. Anderson[2]

AFFILIATIONS

[1]Korea Institute of Fusion Energy (KFE), Daejeon 34133, South Korea
[2]Department of Space, Earth and Environment Sciences, Chalmers University of Technology, SE-412 96 Göteborg, Sweden

[a)]Author to whom correspondence should be addressed: mleconte@kfe.re.kr

ABSTRACT

Collisionless trapped-electron mode (CTEM) turbulence is an important contributor to heat and particle transport in fusion devices. The ion-temperature gradient (ITG)/trapped-electron mode (TEM) fluid models are rarely treated analytically, due to the large number of transport channels involved, e.g., particle and ion/electron heat transport. The CTEM fluid model [Anderson *et al.*, Plasma Phys. Controlled Fusion **48**, 651 (2006)] provides a simplified model, in the regime where the density gradient drive (∇n) is negligible compared to the electron temperature gradient drive (∇T_e). This provides a starting point to study mechanisms associated with linear waves, such as crossphase dynamics, and its possible role in the formation of $E \times B$ staircase. Here, an extended CTEM fluid model (with both ∇n and ∇T_e drive) is derived from the more general ITG/TEM model, using a simplified ion density response, and its linear dynamics is first analyzed and compared with CTEM gyrokinetic simulations with bounce-averaged kinetic electrons, while nonlinear analysis is left for future work. The wave action density is derived for this CTEM model. Comparisons of linear ITG spectrum are also made with other analytical models.

I. INTRODUCTION

In magnetic fusion devices, electron heat transport and particle transport is partly due to collisionless trapped-electron mode (CTEM) turbulence, which is usually coupled to ion-temperature gradient (ITG) turbulence. For a review on turbulent particle transport, see, e.g., Refs. 1–3. The CTEM is an instability due to the toroidal precession-drift resonance of trapped electrons in the low-collisionality regime.[4] It is driven by electron temperature gradient and/or density gradient. The Chalmers model[5–10] provides a simple yet predictive set of fluid models for ITG and CTEM turbulence. This set of models has been linearly analyzed. However, there remain certain aspects that are not fully understood, such as the crossphase dynamics responsible for the transport.[11–14] Here, by "crossphase dynamics," we mean the fast transient change in the value of the transport crossphase (e.g., between fluctuating density and potential for particle transport). In other words, this is the study of the departure of the crossphase from its phase-locked value typically assumed in the $i\delta$ approximation. Linear and quasi-linear transport theory often assumes that if the instability is above its linear threshold, then turbulent transport automatically ensues. However, there is a possibility that the crossphase either does not lock, or that it locks to a value different from the one predicted by linear theory. For example, zonal profiles of density and temperature may have an effect on the crossphase.[11] This effect could be particularly important near marginality, where zonal flow and zonal profiles can be significant. In this article, we first analyze the ITG–trapped-electron mode (TEM) model linearly—including the crossphase dynamics. Focusing on the limit of CTEM, we extend the two-field model of Ref. 10 to include the density gradient drive (∇n). This extended CTEM model is compared to linear gyrokinetic simulations with bounce-averaged kinetic electrons.[15] This article reports results that can be considered a first step toward the later goal of better interpreting aspects of nonlinear physics. More precisely, a weakly nonlinear extension of the present work could be used to analyze zonal density and zonal electron temperature corrugations associated with zonal staircase with nonlinear simulations,[16–19] its relation to zonal flows, and their possible relation to the transport crossphase.[11,12] This is left for future work. Quasi-linear transport analysis—which neglects zonal structures—has had some success in comparison with experiments.[20] However, near marginal-stability where zonal structures become dominant players, quasi-linear theory can become inapplicable. Near marginality, analytically tractable fluid models can provide a theoretical basis to understand the interaction between zonal structures

and the background turbulence driving them, e.g., via the wave-kinetic approach.[21,22]

The rest of this article is organized as follows. In Sec. II, we present the general ITG–TEM model used in this study; a linear analysis and general crossphase dynamics analysis is presented. The derivation of the ITG dispersion relation is reviewed and compared to linear gyrokinetic simulations. In Sec. III, we focus on the CTEM, a subset of the ITG–TEM model. The model is analyzed—including the detailed crossphase dynamics—and compared with linear gyrokinetic simulations. In Sec. IV, we discuss the results and present conclusions.

II. MODEL

We are interested in collisionless trapped electron modes (CTEM) for which the frequency verifies $k_\parallel v_{th,i} \ll \omega_k < k_y v_{th,e}$. Although electron trapping is a toroidal phenomenon, we assume a slab geometry, for simplicity. We stress here that the model described in this work only applies to tokamaks, not stellarators. We consider the following fluid model of ITG–TEM turbulence, based on Nordman *et al.*:[7]

$$\frac{\partial n}{\partial t} + \mathbf{v}_E.\nabla n + f_t v_{*e}\frac{\partial \phi}{\partial y} = -\epsilon_n g_e v_{*e}\frac{\partial}{\partial y}(n - f_t\phi + f_t T_{et}), \quad (1)$$

$$\frac{\partial T_{et}}{\partial t} + \mathbf{v}_E.\nabla T_{et} + \eta_e v_{*e}\frac{\partial \phi}{\partial y} = -\frac{\Gamma-1}{f_t}\epsilon_n g_e v_{*e}\frac{\partial}{\partial y}\left(n - f_t\phi + \left(1+\frac{\Gamma}{\Gamma-1}\right)f_t T_{et}\right), \quad (2)$$

$$\left[\frac{\partial}{\partial t} + \mathbf{v}_E.\nabla\right]\left[(1-f_t)\tilde{\phi} - \nabla_\perp^2\phi\right] + \left(1 - f_t + \frac{1+\eta_i}{\tau}\nabla_\perp^2\right)v_{*e}\frac{\partial\phi}{\partial y} = \epsilon_n g_i v_{*e}\frac{\partial}{\partial y}[(1-f_t)(g_e/g_i + 1/\tau)\phi + T_i + (g_e/g_i + 1/\tau)n + (g_e/g_i)f_t T_{et}], \quad (3)$$

$$\frac{\partial T_i}{\partial t} + \mathbf{v}_E.\nabla T_i = -\frac{v_{*e}}{\tau}\left[\eta_i + \frac{\Gamma-1}{\tau}(1+\eta_i+\tau)\nabla_\perp^2\right]\frac{\partial\phi}{\partial y} + \frac{(\Gamma-1)\epsilon_n g_i v_{*e}}{\tau}\frac{\partial}{\partial y}\left[\frac{1}{\tau}(1 - f_t + (g_e/g_i)\tau)\phi_k + \left(1+\frac{\Gamma}{\Gamma-1}\right)T_i + \frac{n}{\tau}\right] + \frac{(\Gamma-1)\epsilon_n g_i v_{*e}}{\tau^2}\nabla_\perp^2\frac{\partial}{\partial y} \times \left[(1+\tau)\phi + \frac{\tau}{1-f_t}T_i + \frac{1+\tau}{1-f_t}n + \frac{f_t\tau}{1-f_t}T_{et}\right]. \quad (4)$$

Equation (1) represents the conservation of effective electron density, Eq. (2) is the electron heat balance, Eq. (3) is charge balance, and Eq. (4) is the ion heat balance. Here, $n = n_{et} + f_t\tilde{\phi}$ is an effective density, with $n_{et} = \int d^3v\, h_e/n_0$ the trapped electron density.[23,24] Here, h_e is the trapped-electron part of the electron distribution function. The effective density is such that it can be written in the form: $\frac{n}{f_t} = \tilde{\phi} + \frac{n_{et}}{f_t}$, i.e., as the sum of an adiabatic component plus a non-adiabatic component due to trapped electrons. Note that this convention for trapped electrons is a different convention than the one used in the Chalmers model. Namely, in the present model, quasi-neutrality reads $n_i = n + (1-f_t)\tilde{\phi}$, since passing electrons are assumed adiabatic. However, Eqs. (1), (2), (3), and (4) practically correspond to Eqs. (5), (6), (1) + (7), and (2), respectively, of Ref. 7. The quantity ϕ denotes the electric potential, $\tilde{\phi} = \phi - \langle\phi\rangle$, with $\langle\cdot\rangle = \frac{1}{L_y}\int dy$ the flux surface average, and $\mathbf{v}_E = \hat{z}\times\nabla\phi$ denotes the $E\times B$ drift (the magnetic field factor B is absorbed in the normalizations). The electric potential is normalized as $\frac{e\phi}{T_{e0}} \to \phi$, with T_{e0} a reference electron temperature. The quantity $\nabla_\perp^2 = \frac{\partial^2}{\partial x^2} + \frac{\partial^2}{\partial y^2}$ is the perpendicular Laplacian, and x, y, and z denote the local radial, poloidal, and toroidal directions in a fusion device. Time is normalized as $(c_s/L_n)t \to t$, with $c_s = \sqrt{T_e/m_i}$ the sound speed, and space is normalized by the gyroradius at the electron temperature $\rho_s = c_s/\omega_{c,i}$, with $\omega_{c,i} = eB/m_i$ the ion gyrofrequency. Here, $L_n = n/|\nabla n|$ is the density gradient scale length, and the parameters η_e, η_i are normalized gradient ratios, given by $\eta_a = \frac{L_n}{L_{Ta}} = \frac{n}{T_a}\frac{|\nabla T_a|}{|\nabla n|}$, with $a = e, i$. The quantity $\tau = T_{e0}/T_{i0}$ is the temperature ratio, and $\Gamma = 5/3$ is the adiabatic index. The parameter $f_t = \sqrt{\epsilon}$ is the trapped-electron fraction, with $\epsilon = a/R$ the inverse aspect ratio, and terms proportional to $\epsilon_n = 2L_n/R$ denote magnetic drift effects modeling magnetic drift for ions and toroidal precession-drift for trapped-electrons. The parameter $g_e(s) = \frac{1}{4} + \frac{2}{3}s$ represents the effect of magnetic shear on the precession frequency of trapped-electrons, and $g_i(s) = \frac{2}{3} + \frac{5}{9}s - \epsilon$ is its effect on the magnetic drift for ions.[25,26] Since we are interested in frequencies $\omega \gg k_\parallel c_s$, where c_s is the sound speed, we neglect parallel ion motion.

A. ITG–TEM system

In this section, we neglect magnetic shear effects, i.e., we assume $g_i = g_e = 1$, for simplicity. Later on, we will focus on CTEM. That is, considering quasi-neutrality in the form $n_i^{GC} = n + (1 - f_t - \nabla_\perp^2)\times[\phi - \langle\phi\rangle]$, with n_i^{GC} the ion gyrocenter density, we assume that the mode frequency resonates with the precession-drift frequency, i.e., $\omega_k \sim \frac{5}{3}\omega_{de}$, where ω_k is the mode frequency at wavenumber $\mathbf{k}$, $\omega_{de} = k_y\epsilon_n v_{*e}$ is the toroidal precession drift frequency, with k_y the poloidal wavenumber. Hence, we use the approximation:

$$\omega_k - \omega_{di} \simeq \omega_k, \quad T_{ik} \sim 0, \quad (5)$$

where $\omega_{di} = -k_y\epsilon_n v_{*e}/\tau$ is the ion magnetic drift (sum of ∇B and curvature drifts), and T_{ik} denotes the Fourier amplitude of ion temperature fluctuations. In this regime, the electron dynamics decouples from the ion dynamics, and the nominally quartic dispersion relation reduces to a cubic, which can be analytically solved. The present CTEM model is an extension of the two-field model of Ref. 10, to include the ion dynamics, although in a simplified form. This is important, because CTEM is an ion-scale mode. Hence, polarization—ion inertia—and ion finite-Larmor-radius (FLR) stabilization effects are important for this mode. Note that, although $|T_{ik}| \sim 0$ is assumed, this is only for the amplitude of fluctuations. There is still a large value of the equilibrium ion temperature $T_{i0} \neq 0$; hence, FLR and polarization effects are retained.

B. Linear analysis

Linearizing systems (1)–(4), and applying a Fourier transform $g = g_k(t)e^{ik_x x + ik_y y}$, with $g = n_i, n, T_{et}, \phi$, one obtains—after some algebra—the following ITG–TEM linear dispersion relation ($\omega_* = k_y v_{*e}$):

$$\frac{(\omega_* + \tau\omega_{di})\left(\omega - \frac{5}{3}\omega_{di}\right) - k_\perp^2\left(\omega + \frac{1+\eta_i}{\tau}\omega_*\right)\left(\omega - \frac{5}{3}\omega_{di}\right) + \left(\eta_i - \frac{2}{3}\right)\omega_*\omega_{di}}{N_i}$$
$$= f_t \frac{(\omega_* - \omega_{de})\left(\omega - \frac{5}{3}\omega_{de}\right) + \left(\eta_e - \frac{2}{3}\right)\omega_*\omega_{de}}{N_e} + 1 - f_t, \tag{6}$$

where the denominators are $N_i = \omega^2 - \frac{10}{3}\omega_{di}\omega + \frac{5}{3}\omega_{di}^2$ and $N_e = \omega^2 - \frac{10}{3}\omega_{de}\omega + \frac{5}{3}\omega_{de}^2$. The details of the derivation are given in the Appendix. The relation (6) is a quartic dispersion relation that describes two coupled modes: an electron mode (CTEM rotating in the electron diamagnetic direction) and an ion mode (ITG rotating in the ion diamagnetic direction).[10] As we focus here on trapped electron mode turbulence, we assume $\eta_i \ll \eta_e$, and thus the electron branch (CTEM branch) is dominant. In the CTEM regime, $|N_i| \gg |N_e|$. Hence, the CTEM mode resonates at the frequency $\omega_k = \omega_{\rm res} = \frac{5}{3}\omega_{de}$. We are talking here about a fluid resonance, which is an approximation of the kinetic resonance.[5] To see the quasi-symmetry between ITG and TEM, it is useful to write the ITG–TEM system in matrix form,

$$\begin{bmatrix} \omega - \frac{5}{3}\omega_{de} & -\frac{2}{3f_t}\omega + \left(\eta_e - \frac{2}{3}\right)\frac{\omega_*}{1-f_t} & -\left(\eta_e - \frac{2}{3}\right)\frac{\omega_*}{1-f_t} & 0 \\ -f_t\omega_{de} & \omega - \omega_{de} + \Lambda_k^{\rm TEM} & -\Lambda_k^{\rm TEM} & 0 \\ 0 & \Lambda_k^{\rm ITG}(\omega) & \omega - \omega_{di} - \Lambda_k^{\rm ITG}(\omega) & -\tau\omega_{di} \\ 0 & \left(\eta_i - \frac{2}{3}\right)\frac{\omega_*/\tau}{1-f_t} & -\frac{2}{3\tau}\omega - \left[\left(\eta_i - \frac{2}{3}\right)\frac{\omega_*/\tau}{1-f_t}\right] & \omega - \frac{5}{3}\omega_{di} \end{bmatrix} \begin{bmatrix} T_{ek} \\ n_k \\ n_{ik} \\ T_{ik} \end{bmatrix} = 0, \tag{7}$$

where we used quasi-neutrality to express the electric potential: $\phi_k = \frac{1}{1-f_t}(n_{ik} - n_k)$, the parameters $\Lambda_k^{\rm TEM} = \xi(\omega_* - \omega_{de})$ and $\Lambda_k^{\rm ITG}(\omega) = \frac{1}{1-f_t}\left[\left(1 - \frac{1+\eta_i}{\tau}k_\perp^2\right)\omega_* + \tau\omega_{di} - k_\perp^2\omega\right]$ were defined, and $\xi = f_t/(1-f_t)$. This form of the ITG–TEM system clearly shows that the system is almost block-diagonal, with the coupling between the two branches occurring only through the effective electron density n_k and the ion density n_{ik}.

The two branches decouple in the following two limits: (i) The toroidal ITG mode is recovered in the limit of negligible trapped electron fraction $f_t \to 0$ corresponding to Boltzmann electrons, for which the effective electron density is negligible $|n_k| \ll |n_{ik}|, |T_{ik}|$. It corresponds to the lower block-diagonal in Eq. (7). Note that the total electron density in this case is simply $n_{ek} = n_{ik} \simeq \phi_k$. (ii) The CTEM is recovered in the limit $\omega_k - \omega_{di} \sim \omega_k$, and $|T_{ik}| \ll |T_{ek}|, |\phi_k|$. It corresponds to a sub-set of the 3×3 upper sub-matrix in Eq. (7).

An alternative way to represent the system is in terms of the ion gyrocenter density $n_i^{\rm GC} = n_i - \nabla_\perp^2\phi$ instead of ion density n_i. Then, the electric potential is given by $\phi_k = \frac{1}{1-f_t+k_\perp^2}(n_{ik}^{\rm GC} - n_k)$, and the system can be written in the form of the following Schrödinger-like equation:

$$i\frac{\partial}{\partial t}\Psi = \begin{bmatrix} \frac{5}{3}\omega_{de} & -\left[\left(\eta_e - \frac{2}{3}\right)\frac{\omega_*}{1-f_t+k_\perp^2} - \frac{10}{9f_t}\omega_{de}\right] & \left(\eta_e - \frac{2}{3}\right)\frac{\omega_*}{1-f_t+k_\perp^2} & 0 \\ f_t\omega_{de} & \frac{5}{3}\omega_{de} - \Lambda_k^{\rm TEM} & \Lambda_k^{\rm TEM} & 0 \\ 0 & -\Lambda_k^{\rm GC} & \frac{5}{3}\omega_{di} + \Lambda_k^{\rm GC} & \tau\omega_{di} \\ 0 & -\left(\eta_i - \frac{2}{3}\right)\frac{\omega_*/\tau}{1-f_t+k_\perp^2} & \left(\eta_i - \frac{2}{3}\right)\frac{\omega_*/\tau}{1-f_t+k_\perp^2} + \frac{10}{9\tau}\omega_{di} & \frac{5}{3}\omega_{di} \end{bmatrix}\Psi. \tag{8}$$

The following quantities were introduced:

$$s_{ik} = T_{ik} - \frac{2}{3\tau}n_{ik} \quad \text{and} \quad s_{ek} = T_{ek} - \frac{2}{3f_t}n_k, \tag{9}$$

where s_{ik} (s_{ek}) is the thermodynamic entropy for ions (electrons), as described for ITG in Refs. 27 and 28. Here, $\Psi = [s_{ek}, n_k, n_{ik}^{\rm GC}, s_{ik}]^T$ is the eigenvector, the coefficient $\Lambda_k^{\rm ITG}(\omega)$ is now replaced by $\Lambda_k^{\rm GC} = \frac{1}{1-f_t+k_\perp^2}\left[\left(1 - \frac{1+\eta_i}{\tau}k_\perp^2\right)\omega_* + \tau\omega_{di} - \frac{5}{3}k_\perp^2\omega_{di}\right]$ which does not depend on the complex frequency ω, and $\Lambda_k^{\rm TEM}$ is now defined as $\Lambda_k^{\rm TEM} = \xi_k(\omega_* - \omega_{de})$, where the trapping parameter ξ_k is defined as

$$\xi_k = \frac{f_t}{1-f_t+k_\perp^2}. \tag{10}$$

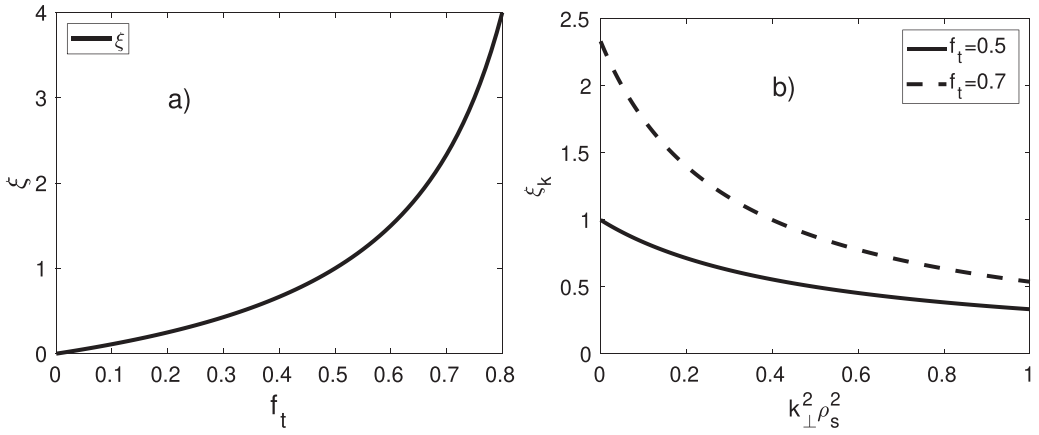

FIG. 1. Parameter $\xi_k = f_t/(1 - f_t + k_\perp^2)$ vs (a) trapped-fraction f_t for $k_\perp^2 = 0$, and (b) square wavenumber $k_\perp^2$ for two values of $f_t = 0.5$ (solid) and 0.7 (dash).

It depends on the squared wavenumber $k_\perp^2$, which represents polarization effects. The ratio ξ_k is shown vs trapped-fraction f_t for $k_\perp^2 = 0$ [Fig. 1(a)]. One sees that the parameter ξ_k is of order unity for $f_t \simeq 0.5$ and increases rapidly for $f_t > 0.5$. This parameter is also shown vs square wavenumber $k_\perp^2$ for two values of $f_t = 0.5$ and 0.7 [Fig. 1(b)].

The Schrödinger-like equation (8) will be useful, in a future work, for deriving the wave-kinetic equation (WKE) and studying the nonlinear coupling of turbulence to zonal modes.

C. Crossphase dynamics

To analyze the crossphase dynamics, it is convenient to re-write Eq. (8) in terms of $s_{ek}, n_k, n_{ik}, s_{ik}$ and the electric potential ϕ_k

$$\left(\omega - \frac{5}{3}\omega_{de}\right)s_{ek} - \left(\eta_e - \frac{2}{3}\right)\omega_* \phi_k - \frac{10}{9f_t}\omega_{de} n_k = 0, \tag{11}$$

$$\left[\omega - \frac{5}{3}\omega_{de}\right]n_k - f_t\omega_{de}s_{ek} - f_t(\omega_* - \omega_{de})\phi_k = 0, \tag{12}$$

$$\left[\omega - \frac{5}{3}\omega_{di}\right]n_{ik} - \tau\omega_{di}s_{ik} - (\omega_* + \tau\omega_{di})\phi_k = 0, \tag{13}$$

$$\left(\omega - \frac{5}{3}\omega_{di}\right)s_{ik} - \left[\left(\eta_i - \frac{2}{3\tau}\right)\omega_*\right]\phi_k + \frac{10}{9\tau}\omega_{di} n_{ik} = 0. \tag{14}$$

Here, the polarization and ion FLR effects are neglected, for simplicity.

Let us define the three crossphases associated with Eqs. (11), (13), and (14):

$$\chi_k = \arg\left(\frac{\phi_k}{s_{ek}}\right), \quad \theta_k = \arg\left(\frac{\phi_k}{n_{ik}}\right), \quad \zeta_k = \arg\left(\frac{\phi_k}{s_{ik}}\right). \tag{15}$$

Note that the crossphase between n_k (representing trapped-electron) and ϕ_k is also equal to θ_k due to the quasi-neutrality condition:

$$n_{ik} = n_k + (1 - f_t)\phi_k. \tag{16}$$

With these definitions, the turbulent particle flux is $\Gamma = \sum_k k_y |n_{ik}||\phi_k| \sin\theta_k$, and the electron/ion entropy fluxes are $\sum_k k_y |s_{ek}||\phi_k| \sin\chi_k$ and $\sum_k k_y |s_{ik}||\phi_k| \sin\zeta_k$, respectively. The ion and electron entropy fluxes are related to the ion and electron heat fluxes $Q_{e,i}$ via $\sum_k k_y \mathrm{Im}\,\phi_k^* s_{ek} = Q_e - \frac{2}{3f_t}\Gamma$ and $\sum_k k_y \mathrm{Im}\,\phi_k^* s_{ik} = Q_i - \frac{2}{3\tau}\Gamma$, where use has been made of the quasi-neutrality condition (16).

We use the following ansatz

$$\begin{bmatrix} \phi_k \\ s_{ek} \\ n_{ik} \\ s_{ik} \end{bmatrix} = \begin{bmatrix} |\phi_k| \\ |s_{ek}|e^{-i\chi_k} \\ |n_{ik}|e^{-i\theta_k} \\ |s_{ik}|e^{-i\zeta_k} \end{bmatrix} e^{-i\omega_k t}, \tag{17}$$

where ω_k is the linear mode frequency.

Replacing s_{ek}, n_k, n_{ik}, and s_{ik} in Eqs. (11), (13), (14), using the ansatz (17), one obtains, after some algebra, the following system:

$$-i|s_{ek}|e^{-i\chi_k}\left[\frac{\partial\chi_k}{\partial t} + \omega_k\right] + \gamma_k e^{-i\chi_k}|s_{ek}|$$
$$= -\frac{5}{3}i\omega_{de}|s_{ek}|e^{-i\chi_k} - i\left(\eta_e - \frac{2}{3}\right)\omega_*|\phi_k| - i\frac{10}{9f_t}\omega_{de}|n_{ik}|e^{-i\theta_k}, \tag{18}$$

$$-i|n_{ik}|e^{-i\theta_k}\left[\frac{\partial\theta_k}{\partial t} + \omega_k\right] + \gamma_k e^{-i\theta_k}|n_{ik}|$$
$$= -\frac{5}{3}i\omega_{de}|n_{ik}|e^{-i\theta_k} - i\tau\omega_{di}|s_{ik}|e^{-i\zeta_k} - i(\omega_* + \tau\omega_{di})|\phi_k|, \tag{19}$$

$$-i|s_{ik}|e^{-i\zeta_k}\left[\frac{\partial\zeta_k}{\partial t} + \omega_k\right] + \gamma_k e^{-i\zeta_k}|s_{ik}|$$
$$= -\frac{5}{3}i\omega_{di}|s_{ik}|e^{-i\zeta_k} - i\left[\left(\eta_i - \frac{2}{3\tau}\right)\omega_* + (1 - f_t)\frac{10}{9\tau}\omega_{di}\right]|\phi_k|$$
$$- i\frac{10}{9\tau}\omega_{di}|n_{ik}|e^{-i\theta_k}, \tag{20}$$

where we used $\partial_t|u_k| = \gamma_k|u_k|$, for $u_k = n_{ik}, s_{ek}, s_{ik}$. It is apparent that Eqs. (19) and (20) can be independently solved from Eq. (18). Physically, the crossphase χ_k responsible for electron thermal transport does not influence the crossphases θ_k and ζ_k associated with ion transport. More precisely, the coupling of ion crossphases to electron crossphases only occurs through the dependence of the amplitude ratios α_k, β_k on the electric potential amplitude $|\phi_k|$, We will thus first solve for the ion crossphases. Once the particle transport crossphase θ_k is known, one can obtain the crossphase dynamics for electron heat transport associated with the crossphase χ_k Eq. (18) in closed form. This will be done in the CTEM limit in Sec. III C. One can separate the

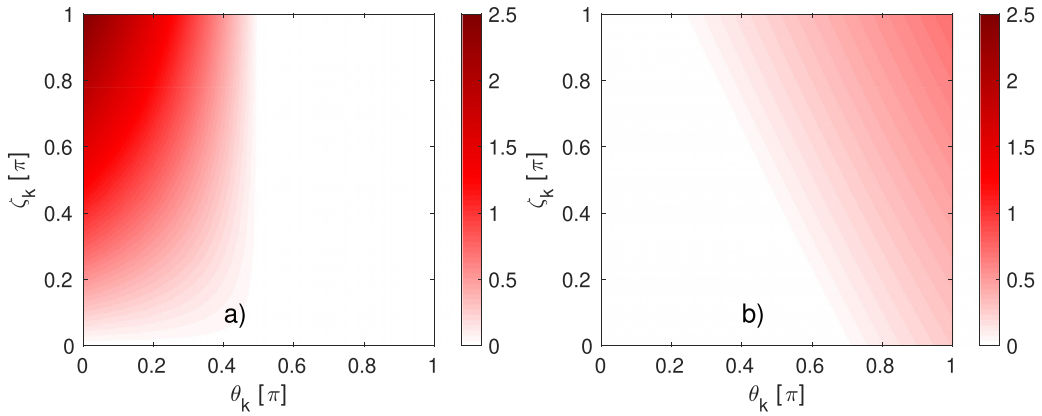

FIG. 2. Amplitude ratios for ITG/TEM: (a) inverse amplitude ratio $A_k = \frac{1}{\alpha_k}$ and (b) $B_k = \frac{1}{\beta_k}$, expressions (28) and (29) vs θ_k and ζ_k, for the parameters $\eta_i = 2$, $\epsilon_n = 0.8$ and $\gamma_k/\omega_* = 1$.

real and imaginary parts of Eqs. (19) and (20). The real part yields two relations between the crossphases θ_k, ζ_k and the linear growth rate:

$$\gamma_k = (\omega_* + \tau\omega_{di})\alpha_k \sin\theta_k + \tau\omega_{di}\frac{\alpha_k}{\beta_k}\sin\psi_k, \tag{21}$$

$$\gamma_k = -\frac{10}{9\tau}\omega_{di}\frac{\beta_k}{\alpha_k}\sin\psi_k + \left(\eta_i - \frac{2}{3}\right)\omega_*\beta_k\sin\zeta_k, \tag{22}$$

where $\gamma_k = |n_{ik}|^{-1}\partial_t|n_{ik}| = |s_{ik}|^{-1}\partial_t|s_{ik}| = |s_{ek}|^{-1}\partial_t|s_{ek}|$ is the linear growth rate, and $\psi_k = \theta_k - \zeta_k$ is the crossphase mismatch responsible for transport decoupling between particle transport vs ion heat transport. The quantities α_k and β_k are the two amplitude ratios defined as

$$\alpha_k = \frac{|\phi_k|}{|n_{ik}|}, \quad \beta_k = \frac{|\phi_k|}{|s_{ik}|}, \tag{23}$$

and $\alpha_k/\beta_k = |s_{ik}|/|n_{ik}|$ is the third amplitude ratio.

The imaginary part of Eqs. (19) and (20) yields the following crossphase dynamics

$$\frac{\partial\theta_k}{\partial t} = \omega_{\rm res} - \omega_k + (\omega_* + \tau\omega_{di})\alpha_k\cos\theta_k + \tau\omega_{di}\frac{\alpha_k}{\beta_k}\cos\psi_k, \tag{24}$$

$$\frac{\partial\zeta_k}{\partial t} = \omega_{\rm res} - \omega_k + \frac{10}{9\tau}\omega_{di}\frac{\beta_k}{\alpha_k}\cos\psi_k + \left(\eta_i - \frac{2}{3}\right)\omega_*\beta_k\cos\zeta_k, \tag{25}$$

$$\frac{\partial\psi_k}{\partial t} = \left(\tau\frac{\alpha_k}{\beta_k} - \frac{10}{9\tau}\frac{\beta_k}{\alpha_k}\right)\omega_{di}\cos\psi_k + (\omega_* + \tau\omega_{di})\alpha_k\cos\theta_k - \left(\eta_i - \frac{2}{3}\right)\omega_*\beta_k\cos\zeta_k, \tag{26}$$

where $\omega_{\rm res} = \frac{5}{3}\omega_{di}$ is the ion resonance frequency. Here, Eq. (26) is the difference of Eqs. (24) and (25). Considering the amplitude ratio system (21) and (22), it is convenient to define the inverse amplitude ratios $A_k = 1/\alpha_k$ and $B_k = 1/\beta_k$. After some algebra, one obtains the following matrix system:

$$\begin{bmatrix} \gamma_k & \tau\omega_{di}\sin\psi_k \\ -\frac{10}{9\tau}\omega_{di}\sin\psi_k & \gamma_k \end{bmatrix}\begin{bmatrix} A_k \\ B_k \end{bmatrix} = \begin{bmatrix} (\omega_* + \tau\omega_{di})\sin\theta_k \\ \left(\eta_i - \frac{2}{3}\right)\omega_*\sin\zeta_k \end{bmatrix}. \tag{27}$$

Inverting the matrix yields after some algebra

$$\frac{1}{\alpha_k} = \frac{[(1-\epsilon_n)\omega_*/\gamma_k]\sin\theta_k - \tau\left(\eta_i - \frac{2}{3}\right)(\epsilon_n{\omega_*}^2/{\gamma_k}^2)\sin\zeta_k\sin\psi_k}{1 + \frac{10}{9}\epsilon_n^2({\omega_*}^2/{\gamma_k}^2)\sin^2\psi_k}, \tag{28}$$

$$\frac{1}{\beta_k} = \frac{\left(\eta_i - \frac{2}{3}\right)(\omega_*/\gamma_k)\sin\zeta_k + \frac{10}{9}\left[(1-\epsilon_n)\epsilon_n{\omega_*}^2/{\gamma_k}^2\right]\sin\theta_k\sin\psi_k}{1 + \frac{10}{9}\epsilon_n^2({\omega_*}^2/{\gamma_k}^2)\sin^2\psi_k}. \tag{29}$$

The inverse amplitude ratios A_k and B_k, expressions (28) and (29) are plotted vs θ_k and ζ_k, for the parameters $\eta_i = 2$, $\epsilon_n = 0.8$, $\tau = 1$, and $\gamma_k/\omega_* = 1$ (Fig. 2). Values on the forbidden domains—since A_k and B_k are amplitudes, they must be positive—are set to zero for clarity.

Alternatively, this can also be written

$$\alpha_k = \frac{\gamma_k/\omega_*}{(1-\epsilon_n)\sin\theta_k + \frac{1}{\beta_k}\tau\epsilon_n\sin\psi_k}, \tag{30}$$

$$\beta_k = \frac{\gamma_k/\omega_*}{\left(\eta_i - \frac{2}{3}\right)\sin\chi_k - \frac{1}{\alpha_k}\cdot\frac{10}{9\tau}\epsilon_n\sin\psi_k}. \tag{31}$$

It is clear from Eqs. (30) and (31) that the two amplitude ratios α_k and β_k are coupled. One identifies two opposite regimes: $\frac{1}{\beta_k} \ll 1$, corresponding to negligible ion heat transport (i.e., $|T_{ik}| \ll 1$), and $\frac{1}{\alpha_k} \ll 1$ corresponding to negligible particle transport. In the following, we will focus on the former case, since our main focus is on analytically understanding CTEM turbulence. It is well known that experimentally, in present tokamaks, it is mainly the role of trapped-electrons in ITG-driven turbulence that produces the electron particle transport.[1–3] However, from a theoretical point of view, it is easier to separate the two branches, by saying that we deal with TEM whenever trapped-electrons are included. In this picture, the ITG-driven particle transport due to trapped-electrons is recast as a "mixed-mode" due to coupling of the ITG and TEM branches. In the regime $\frac{1}{\beta_k} \ll 1$, the turbulence

corresponds to CTEM. In this regime, one may neglect the coupling of the amplitude ratio α_k to β_k, i.e., one uses the approximation:

$$\alpha_k \simeq \frac{\gamma_k}{(\omega_* + \tau\omega_{di})\sin\theta_k}. \tag{32}$$

Then, the dynamics of the density–potential crossphase θ_k decouples from the other crossphases ζ_k and ψ_k, and reduces to:

$$\frac{\partial\theta_k}{\partial t} \simeq -(\omega_k - \omega_{\rm res}) + \gamma_k \cot\theta_k, \tag{33}$$

where $\cot\zeta_k = 1/\tan\zeta_k$ is the cotangent of the crossphase. This shows that the crossphase responsible for particle transport locks to an averaged value θ_k^0 related to the CTEM linear growth rate via:

$$\theta_k^0 = \text{atan}\left[\frac{\gamma_k}{\omega_k - \omega_{\rm res}}\right]. \tag{34}$$

The advantage of working with the crossphase dynamics, compared with the standard analysis of transport based on averaged crossphase, is that the present analysis can be extended to include the effects of zonal modes on the transport crossphase.[11] This is left for future work.

D. ITG limit

Linearizing the original ITG–TEM system (1)–(4), one obtains

$$-i\omega n_k + if_t\omega_*\phi_k = -i\epsilon_n g_e\omega_*(n_k - f_t\phi_k + f_t T_{ek}), \tag{35}$$

$$-i\omega T_{ek} + i\eta_e\omega_*\phi_k = -\frac{2}{3f_t}i\epsilon_n g_e\omega_*\left(n_k - f_t\phi_k + \frac{7}{2}f_t T_{ek}\right), \tag{36}$$

$$\begin{aligned}-(1-f_t+k_\perp^2)i\omega\phi_k + i\left(1 - f_t - \frac{1+\eta_i}{\tau}k_\perp^2\right)\omega_*\phi_k \\ = i\epsilon_n g_e\omega_*[(1-f_t)(1+g_i/(g_e\tau))\phi_k + (g_i/g_e)T_{ik} \\ +(1+g_i/(g_e\tau))n_k + f_t T_{ek}],\end{aligned} \tag{37}$$

$$\begin{aligned}-i\omega T_{ik} = i\frac{\epsilon_n g_e\omega_*}{\tau}\left[\frac{2}{3\tau}(1-f_t+\tau)\phi_k + \frac{2}{3\tau}n_k + \frac{7}{3}T_{ik}\right] \\ -i\left[\eta_i - \frac{2}{3\tau}(1+\eta_i+\tau)k_\perp^2\right]\frac{\omega_*}{\tau}\phi_k \\ -\frac{2}{3\tau^2}ik_\perp^2\epsilon_n g_e\omega_*\left[(1+\tau)\phi_k + \frac{\tau}{1-f_t}T_{ik} + \frac{1+\tau}{1-f_t}n_k + \frac{\tau f_t}{1-f_t}T_{ek}\right].\end{aligned} \tag{38}$$

The linear dispersion relation is best obtained by first transforming the system. Adding Eqs. (35) and (37) yields the ion continuity equation:

$$\begin{aligned}-i\omega(n_{ik} + k_\perp^2\phi_k) + \left(1 - \frac{1+\eta_i}{\tau}k_\perp^2\right)i\omega_*\phi_k \\ = i\frac{\epsilon_n g_i\omega_*}{\tau}[(1-f_t+\tau)\phi_k + n_k + \tau T_{ik}],\end{aligned} \tag{39}$$

where $n_{ik} = n_k + (1-f_t)\phi_k$ is the ion density perturbation set by quasi-neutrality (this is the particle—not gyrocenter—density). In the ITG limit, i.e., without trapped-electrons $f_t \to 0$, the ion continuity equation and ion heat balance become:

$$\begin{aligned}-i\omega(n_{ik} + k_\perp^2\phi_k) + \left(1 - \frac{1+\eta_i}{\tau}k_\perp^2\right)i\omega_*\phi_k \\ = i\frac{\epsilon_n g_i\omega_*}{\tau}[(1+\tau)\phi_k + n_{ik} + \tau T_{ik}],\end{aligned} \tag{40}$$

$$\left(-i\omega - i\frac{5}{3}\frac{\epsilon_n g_i\omega_*}{\tau}\right)T_{ik} + \frac{2}{3\tau}i\omega n_{ik} = \frac{2}{3\tau}\left(\eta_i - \frac{2}{3}\right)i\omega_*\phi_k. \tag{41}$$

Defining $\tau_i = T_i/T_e = 1/\tau$, the ion continuity Eq. (40) and ion heat balance Eq. (41) become, respectively,

$$\begin{aligned}-i\omega n_{ik} + (-i\omega - i\alpha_i k_y)k_\perp^2\phi_k + ik_y\phi_k \\ -i\tau_i\epsilon_n g_i k_y\left[\left(1 + \frac{1}{\tau_i}\right)\phi_k + n_{ik} + \frac{T_{ik}}{\tau_i}\right] = 0,\end{aligned} \tag{42}$$

$$-i\omega T_{ik} - ik_y\frac{5}{3}\tau_i\epsilon_n g_i T_{ik} + \left(\eta_i - \frac{2}{3}\right)i\tau_i k_y\phi_k + \frac{2}{3}i\tau_i\omega n_{ik} = 0 \tag{43}$$

with $\alpha_i = \tau_i(1+\eta_i)$. Here, the fields have been further normalized as $n_{ik} \to \frac{L_n}{\rho_s}n_{ik}$, and same for T_{ik}. In the present analytical limit for the description of the ITG instability, electrons are assumed to have a Boltzmann response: $n_{ik} = \phi_k$. From Eq. (43), one obtains after some algebra the following linear response of ion temperature to potential:

$$T_{ik} = \frac{\left(\eta_i - \frac{2}{3}\right)\tau_i k_y + \frac{2}{3}\tau_i\omega}{\omega + \frac{5}{3}\tau_i\epsilon_n g_i k_y}\phi_k. \tag{44}$$

Replacing T_{ik} in Eq. (42) using the response (44), one obtains—after some algebra—the following quadratic dispersion relation:

$$A\omega^2 + B\omega + C = 0 \tag{45}$$

with real-valued coefficients given by $A = 1 + k_\perp^2$, $B = 2k_y\left[\frac{5}{3}\tau_i\epsilon_n g_i - \frac{1}{2}(1-\epsilon_n g_i) + \frac{k_\perp^2}{2}\left(\alpha_i + \frac{5}{3}\tau_i\epsilon_n g_i\right)\right]$ and $C = \tau_i\epsilon_n g_i k_y^2\left[\eta_i - \frac{7}{3} + \frac{5}{3}(1+\tau_i)\epsilon_n g_i + \frac{5}{3}\alpha_i k_\perp^2\right]$. The solution to the ITG dispersion relation (45) is then

$$\omega_{1,2} \simeq -\frac{B}{2A} \pm \frac{1}{2A}\sqrt{B^2 - 4AC}. \tag{46}$$

The unstable branch has a growth rate $\gamma_k \simeq \frac{1}{\sqrt{A}}\sqrt{C - \frac{B^2}{4A}} = \frac{1}{\sqrt{A}}\sqrt{C - A\left(\frac{B}{2A}\right)^2}$. After some algebra, the ITG frequency and growth rate are given by

$$\omega_k^{\rm ITG} \simeq \frac{-k_y}{1+k_\perp^2}\left[\frac{5}{3}\tau_i\epsilon_n g_i - \frac{1}{2}(1-\epsilon_n g_i) + \frac{k_\perp^2}{2}\left(\alpha_i + \frac{5}{3}\tau_i\epsilon_n g_i\right)\right], \tag{47}$$

$$\gamma_k^{\rm ITG} \simeq \frac{k_y\sqrt{\tau_i\epsilon_n g_i}}{\sqrt{1+k_\perp^2}}\sqrt{\eta_i - \eta_i^c}, \tag{48}$$

where $\eta_i^c = \frac{1}{\tau_i\epsilon_n g_i}(1+k_\perp^2)\frac{\omega_k^2}{k_y^2} + \frac{7}{3} - \frac{5}{3}(1+\tau_i)\epsilon_n g_i - \frac{5}{3}\alpha_i k_\perp^2$ is the linear ITG threshold, with $\omega_k = \omega_k^{\rm ITG}$.[29] Note that here the growth rate has a factor $\sqrt{1+k_\perp^2}$ in the denominator, compared to the factor $(1+k_\perp^2)$ in Ref. 29. We believe there was a typo in Ref. 29. The analytic expressions for the real ITG frequency (47) and growth rate (48)

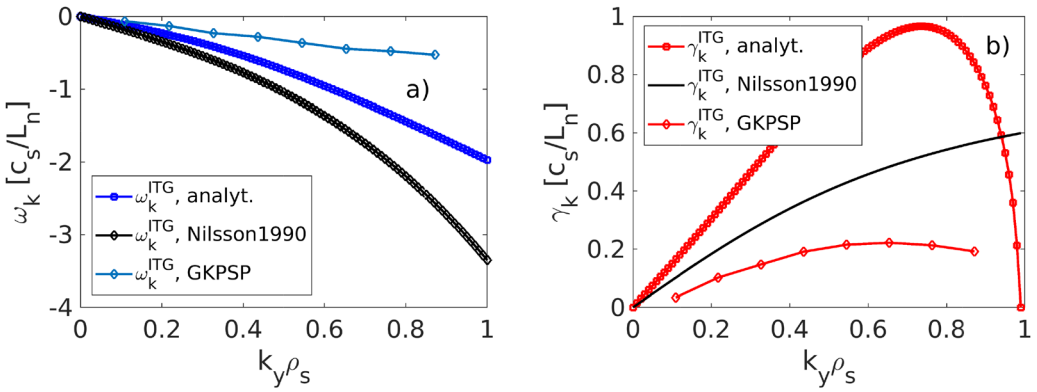

FIG. 3. Comparison of the analytical model with Nilsson *et al.*8 and with gyrokinetic simulations: (a) ITG frequency and (b) ITG growth rate vs poloidal wavenumber k_y. The parameters are $\eta_i = 3$, $\epsilon_n = 1$ ($\frac{R}{L_n} = 2$), $T_i/T_e = 1$, and $\eta_e \simeq 0$, with Boltzmann electrons.

are compared to Eqs. (13b) and (13c) in Nilsson *et al.*,[8] and to linear gyrokinetic simulations with the global gyrokinetic code GKPSP which includes fully gyrokinetic ions and bounce-averaged kinetic electrons.[15] Here, Boltzmann electrons are used for the comparison. To take into account magnetic shear effects, the perpendicular wavenumber $k_\perp^2$ is replaced by its average over a ballooning trial function, yielding $\langle k_\perp^2 \rangle = [1 + (\pi^2 - 7.5)s^2/3]k_y^2$.[30] The parameters are $R/L_n = 2$, $R/L_{Ti} = 6$, $R/L_{Te} \simeq 0$, and $T_i/T_e = 1$. The safety factor is $q = 1.34$ and the magnetic shear $s = 0.75$. The ITG frequency given by expression (47) is plotted vs k_y (squares) and compared to the GKPSP result (diamonds) and to the analytical expression (13b) of Nilsson *et al.*[8] [Fig. 3(a)]. The frequency of the ITG fluid model only shows qualitative similarity with the GKPSP data, but our analytical result shows better agreement with GKPSP data than Ref. 8, especially at large $k_y\rho_s$. This is probably due to the different treatment of ion FLR effects.

The ITG growth rate given by expression (48) is plotted vs k_y (squares) and compared to the Nilsson expression (13c) in Ref. 8 (black), and to the GKPSP result (diamonds) [Fig. 3(b)]. The growth rate also shows qualitative similarity, although the growth rate of the fluid model is much larger than the GKPSP result and peaks at a slightly higher wavenumber. The result from Ref. 8 seems to show closer agreement with the GKPSP data at small $k_y\rho_s$. However, the growth rate peaks at $k_y\rho_s > 1$, which is unphysical. This shows that the formula of Ref. 8 is only valid for $k_y\rho_s \ll 1$.

We also plot the ITG growth rate—normalized to ω_*—vs the parameter ϵ_n (Fig. 4), in the case $\eta_i = 2$, $k_\perp^2 = 0$, and $\tau_i = 1$. Previous analytical results are also plotted, for comparison. In particular, in the Introduction section of Beer's Ph.D. thesis,[31] the ITG growth rate from a "simple fluid" model is compared to results from the "3 + 1 Gyro-Landau-Fluid" model. We cannot compare our results to the latter, as we do not have access to these data, but a comparison is made with the simple fluid case. Note that here, $\epsilon_n = 2L_n/R$ as opposed to L_n/R in Ref. 31. At the value $\epsilon_n \sim 1$—relevant for core plasmas—one can see that expression (48) gives a lower growth rate than the simple fluid model in Ref. 31, and the Jarmen *et al.*[9] formula, which are more consistent with the "gyrofluid" and "kinetic" value of $\gamma/\omega_* \simeq 0.4$ at $\epsilon_n = 1$ in Ref. 31 (not shown). The Nilsson formula from Ref. 8 has even better agreement with the latter results, compared to expression (48).

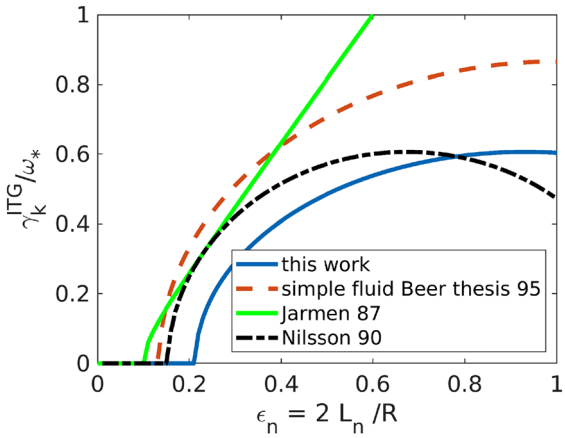

FIG. 4. ITG growth rate vs ϵ_n for the analytical model Eq. (48) (blue) and comparison with three previous analytical models: the simple fluid model from Beer thesis[31] (red), the result from Jarmen *et al.*[9] (green), and by Nilsson *et al.*[8] (black). Other parameters are $\eta_i = 2$, $k_\perp^2 = 0$ and $\tau_i = 1$.

III. CTEM limit

We will now focus on the CTEM. Hence, we use the approximation

$$\omega_k - \omega_{di} \sim \omega_k, \quad \text{and} \quad |T_{ik}| \ll 1. \tag{49}$$

According to the model of Refs. 10 and 25, the electron dynamics totally decouples from the ion dynamics and the ion density fluctuations $|n_{ik}| \ll |n_k|, |\phi_k|$. However, this may be a too strong approximation, since CTEM is ion-scale, so polarization and ion FLR effects are important for this mode. Hence, we may say, instead: for CTEM, the electron dynamics partially decouples from the ion dynamics. In Refs. 10 and 25, the trapped density fluctuations are in-phase with the electric potential fluctuations, which implies no turbulent particle transport, and thus no density-gradient drive for the mode, which is problematic. This is remedied in the present model, where the ion density response is retained, albeit in a simplified form. This directly implies that, in our model, the zonal electron density is present.

The dynamics of zonal density was analyzed for collisional drift-waves in Refs. 11 and 32. Our model should allow to investigate zonal density in the collisionless regime, but this is beyond the scope of this article. Using approximation (49), the system (1)–(4) reduces to the following CTEM model:

$$\frac{\partial n_i}{\partial t}-\frac{\partial^{(i)}\nabla_\perp^2\phi}{\partial t}+\mathbf{v}_E.\nabla n_i-\left(\mathbf{v}_E-\frac{\hat{z}\times\nabla n_i}{\tau}\right).\nabla\nabla_\perp^2\phi + (v_*+\tau v_{\mathrm{di}})\frac{\partial\phi}{\partial y}=0, \tag{50}$$

$$\frac{\partial n}{\partial t}+\mathbf{v}_E.\nabla n+f_t v_*\frac{\partial\phi}{\partial y}=-v_{de}\frac{\partial}{\partial y}(n-f_t\phi+f_t T_{et}), \tag{51}$$

$$\frac{\partial T_{et}}{\partial t}+\mathbf{v}_E.\nabla T_{et}+\eta_e v_{*e}\frac{\partial\phi}{\partial y}=-\frac{2}{3f_t}v_{de}\frac{\partial}{\partial y}\left[n-f_t\phi+\frac{7}{2}f_t T_{et}\right] \tag{52}$$

with $n_i=(1-f_t)\tilde{\phi}+n$, and $\tilde{\phi}=\phi-\langle\phi\rangle$. Here, the operator $\frac{\partial^{(i)}}{\partial t}=\frac{\partial}{\partial t}-\frac{v_*}{\tau}\frac{\partial}{\partial y}$ takes into account ion diamagnetic effects. Note that the connection between the slab geometry of the present model and the standard toroidal action-angle variables is explained in Appendix A of Ref. 28. The simplified CTEM model (50)–(52), which is a limiting case of the original model (1)–(4) also conserves energy.

Linearizing, expressing the potential in terms of effective density n from the quasi-neutrality (16), one obtains the Poisson equation: $(1-f_t-\nabla_\perp^2)\tilde{\phi}=n_i^{\mathrm{GC}}-n$. One obtains, after some algebra,

$$\frac{\partial n_{ik}^{\mathrm{GC}}}{\partial t}+i((1-k_\perp^2/\tau)\omega_*+\tau\omega_{di})\phi_k=0, \tag{53}$$

$$\frac{\partial n_k}{\partial t}+if_t\omega_*\phi_k=-i\omega_{de}[n_k-f_t\phi_k+T_k], \tag{54}$$

$$\frac{\partial T_k}{\partial t}+i\eta_e\omega_*\phi_k=-\frac{2}{3}i\omega_{de}\left[n_k-f_t\phi_k+\frac{7}{2}T_k\right], \tag{55}$$

where $T_k=f_t T_{ek}$, and $\omega_{de}=\epsilon_n g_e\omega_*$ is the trapped-electron precession-drift frequency.

A. Schrödinger-like equation for CTEM

The linear CTEM system can be written in the form of a Schrödinger-like equation. To see this, start with the linearized ion continuity equation of the CTEM model, in the form

$$i\frac{\partial}{\partial t}(n_{ik}+k_\perp^2\phi_k)=\left[\left(1-\frac{k_\perp^2}{\tau}\right)\omega_*+\tau\omega_{di}\right]\phi_k. \tag{56}$$

Using quasi-neutrality, one obtains

$$\begin{aligned} n_{ik}&=(1-f_t)\phi_k+n_k\\ &=(1-f_t+R_k^n)\phi_k, \end{aligned} \tag{57}$$

where $R_k^n=n_k/\phi_k$ is the linear response of effective electron density n_k, given by

$$R_k^n=f_t\frac{(\omega_*-\omega_{de})\left(\omega-\frac{5}{3}\omega_{de}\right)+\left(\eta_e-\frac{2}{3}\right)\omega_*\omega_{de}}{N_e(\omega)}. \tag{58}$$

Here, $N_e(\omega)=\omega^2-\frac{10}{3}\omega_{de}\omega+\frac{5}{3}\omega_{de}^2$, with $\omega=\omega_k+i\gamma_k$ the CTEM eigenfrequency. Note that the normal coordinate $n_{ik}^{\mathrm{GC}}=c_k\phi_k+d_k n_k$, with $c_k=1-f_t+k_\perp^2$, $d_k=1$ can also be obtained following the method of Ref. 33. The ion density can be expressed in the convenient form

$$n_{ik}=(1-f_t+\mathrm{Re}\{R_k^n\})(1-i\tan\theta_k^0), \tag{59}$$

where θ_k^0 is the phase-locked value of the density–potential transport crossphase. For CTEM, it takes the form

$$\theta_k^0=\tan^{-1}\left[\frac{-\mathrm{Im}\{R_k^n\}}{1-f_t+\mathrm{Re}\{R_k^n\}}\right]. \tag{60}$$

Note that in the limit of small transport crossphase $\theta_k^0\to 0$, $\tan\theta_k^0\sim\theta_k^0$, and one recovers the standard $i\delta$ approximation, namely, $n_{ik}\propto 1-i\theta_k^0$.

After some algebra, one obtains the following Schrödinger-like equation:

$$i\frac{\partial}{\partial t}\left[(1-f_t+R_k^n+k_\perp^2)\phi_k\right]=(1-f_t+R_k^n+k_\perp^2)\hat{H}\phi_k, \tag{61}$$

where $\hat{H}$ denotes the Hamiltonian (complex-valued linear frequency), given by

$$\hat{H}=\frac{\left(1-\frac{k_\perp^2}{\tau}\right)\omega_*+\tau\omega_{di}}{(1-f_t+\mathrm{Re}\{R_k^n\})(1-i\tan\theta_k^0)+k_\perp^2}. \tag{62}$$

In the limit $\tau\omega_{di}=-\epsilon_n\omega_*\to 0$, $\frac{1}{\tau}\to 0$, $f_t\to 0$, $R_k^n\to 0$, one recovers the standard textbook drift-wave frequency: $\omega_k\to\omega_*/(1+k_\perp^2)$, as expected. It is convenient to write the Hamiltonian as a sum of Hermitian and anti-Hermitian components:[34]

$$\hat{H}=\hat{H}_H+i\hat{H}_A, \tag{63}$$

where $\hat{H}_H=\frac{1}{2}(\hat{H}+\hat{H}^*)$ is the Hermitian part of the Hamiltonian, and $\hat{H}_A=\frac{1}{2i}(\hat{H}-\hat{H}^*)$ denotes the anti-Hermitian part. Explicitly, one has, for CTEM

$$\hat{H}_H=\frac{(1-f_t+\mathrm{Re}\{R_k^n\}+k_\perp^2)\left[\left(1-\frac{k_\perp^2}{\tau}\right)\omega_*+\tau\omega_{di}\right]}{(1-f_t+\mathrm{Re}\{R_k^n\}+k_\perp^2)^2+(\tan\theta_k^0)^2(1-f_t+\mathrm{Re}\{R_k^n\})^2}, \tag{64}$$

$$\hat{H}_A=\frac{(1-f_t+\mathrm{Re}\{R_k^n\})\left[\left(1-\frac{k_\perp^2}{\tau}\right)\omega_*+\tau\omega_{di}\right]\tan\theta_k^0}{(1-f_t+\mathrm{Re}\{R_k^n\}+k_\perp^2)^2+(\tan\theta_k^0)^2(1-f_t+\mathrm{Re}\{R_k^n\})^2}. \tag{65}$$

Multiplying Eq. (61) by $(1-f_t+R_k^n k_\perp^2)^*$ and symmetrizing, one sees that the *wave action density* for CTEM, takes the form

$$\begin{aligned} W_k&=|1-f_t+R_k^n+k_\perp^2|^2|\phi_k|^2\\ &=\left[(1-f_t+\mathrm{Re}\{R_k^n\}+k_\perp^2)^2+(\mathrm{Im}\{R_k^n\})^2\right]|\phi_k|^2. \end{aligned} \tag{66}$$

Physically, the wave action density is an adiabatic invariant. When the mode frequency varies in time, e.g., due to the increase in the radial wavenumber, i.e., eddy-shearing by zonal flows, the turbulence energy is not conserved. Instead, it is the ratio of turbulence energy E_k to mode frequency, i.e., the wave action density $W_k=E_k/\omega_k$ which is conserved.

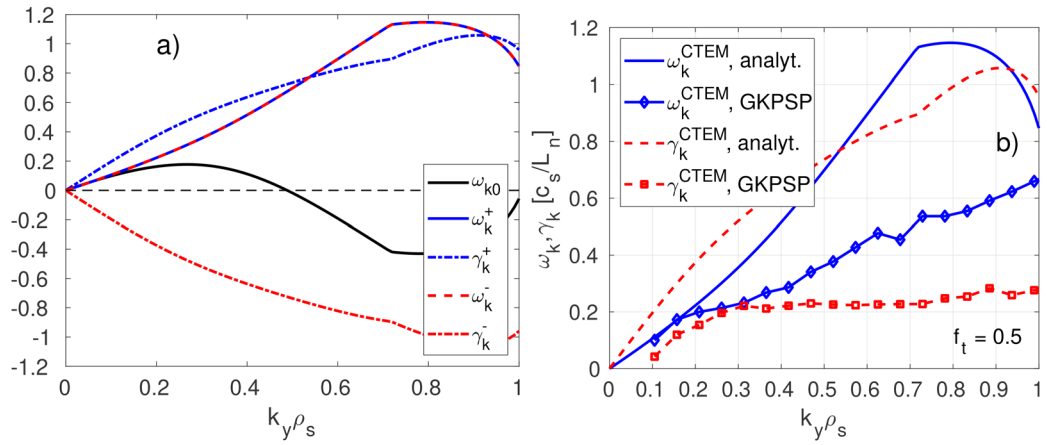

FIG. 5. (a) The three branches of the CTEM cubic dispersion relation ($\omega_k{}^0, \omega_k{}^+, \omega_k{}^-$), and (b) linear growth rate (red) and frequency (blue) of the CTEM unstable branch (solid line), and comparison with GKPSP global gyrokinetic simulations with bounce-kinetic electrons (diamonds). The parameters are $\eta_e = 3.1$ and $\epsilon_n \simeq 0.9$ ($\frac{R}{L_n} = 2.2$). Here, $\eta_i = 1$, $f_t \simeq 0.4$ for the GKPSP simulation, and $\eta_i = 0$, $f_t = 1/2$ for the analytical model.

B. Linear analysis

After some algebra, one obtains the following cubic linear dispersion relation:

$$1 - f_t + k_\perp^2 - \frac{(1-k_\perp^2/\tau)\omega_* + \tau\omega_{di}}{\omega} + f_t \frac{(\omega_* - \omega_{de})\left(\omega - \frac{5}{3}\omega_{de}\right) + \left(\eta_e - \frac{2}{3}\right)\omega_*\omega_{de}}{N_e(\omega)} \simeq 0. \quad (67)$$

Here, the symbol $\simeq$ is used, since the approximate ion density response was considered. The solution for the linearly unstable branch, with $\omega = \omega_k + i\gamma_k$ is

$$\omega_k{}^{\mathrm{CTEM}} = \omega_k{}^0 = \omega_{k0} + \cos\left(\frac{\pi}{3}\right)[|t_k| - s_k], \quad (68)$$

$$\gamma_k{}^{\mathrm{CTEM}} = \sin\left(\frac{\pi}{3}\right)[|t_k| - s_k]. \quad (69)$$

The details are given in Appendix B. The quantities s_k and $|t_k|$ are given by Eqs. (B12) and (B13). For the linearly damped branch, the frequency is $\omega_k{}^{\mathrm{CTEM}}$ and the linear growth rate is $-\gamma_k{}^{\mathrm{CTEM}} < 0$.

The linear frequency (68) and growth rate (69) are shown for the parameters $\eta_e = 3.1$, $f_t = 0.5$ and $\epsilon_n = 2/2.2 \simeq 0.9$, $\eta_i = 0$ (Fig. 5), and compared to linear simulations with the global gyrokinetic code GKPSP.[15] For the GKPSP simulation, the parameters are $\eta_e = 3.1$, $\epsilon_n = 2/2.2$ ($R/L_n = 2.2$), and $\eta_i = 1$. Note that, since GKPSP is a global code (with global profiles), it is not possible to set $\eta_i = 0$ in the code, hence a low but finite value $\eta_i = 1$ was chosen instead.

The CTEM frequency (blue) and growth rate (red) are shown vs normalized poloidal wavenumber $k_y\rho_s$ for the fluid CTEM model (square) and GKPSP linear simulations (diamonds). The fluid CTEM frequency shows only qualitative similarity with the bounce-averaged kinetic result from GKPSP. Namely, both frequencies increase with increasing wavenumber, for $k_y\rho_s < 0.7$. For low wavenumber $k_y\rho_s < 0.2$, the fluid CTEM frequency seems to approximately match the gyrokinetic result. For the growth rate also, there is a large discrepancy between the fluid model compared to the GKPSP result, except for $k_y\rho_s < 0.2$. The fluid CTEM model has a growth rate that increases with $k_y\rho_s$, before reaching a peak at $k_y\rho_s \sim 0.9$ whereas the growth rate becomes almost flat at large $k_y\rho_s$ in the GKPSP simulation. The disagreement shows that there is room for improving the analytical fluid model, but this is left for future work. The discrepancy could be due, in part, to the approximate ion density response used in the analytical model. One way to verify this would be to solve numerically the quartic dispersion-relation associated with the full ITG–TEM fluid model, to check if it resolves some of the discrepancy.

C. CTEM crossphase dynamics

In the present CTEM model, there are only two crossphases: θ_k responsible for particle transport and χ_k associated with electron heat transport. This is because ion heat transport is negligible in this model. We now apply to the CTEM model the same analysis as in Sec. II C. As pointed out in Sec. II C, the dynamics of the density–potential crossphase θ_k in the present CTEM model takes the simple form

$$\frac{\partial\theta_k}{\partial t} = \omega_{\mathrm{res}} - \omega_k + \gamma_k \cot\theta_k. \quad (70)$$

Here, the phase-locked condition $\partial_t\theta_k = 0$ yields the linear crossphase θ_k^0, expression (34) used in quasi-linear particle transport analysis. Hence, the crossphase dynamics for CTEM is similar to the Kuramoto equation for coupled phase-oscillators.[35] In the Kuramoto-like Eq. (70), the first term on the rhs $\omega_{\mathrm{res}} - \omega_k$ is the "entrainment frequency" responsible for *phase-mixing*. Note that $\omega_{\mathrm{res}} = \frac{5}{3}\omega_{de}$, and $\omega_k = \omega_{k0} + \cos\left(\frac{\pi}{3}\right)[|t_k| - s_k]$ for the present CTEM model, with ω_{k0}, s_k and t_k given in Appendix Eqs. (B7), (B12), and (B13). Hence, for CTEM, the entrainment frequency takes the form $\omega_{\mathrm{res}} - \omega_k = \frac{5}{3}\omega_{de} - \omega_{k0} - \cos\left(\frac{\pi}{3}\right)[|t_k| - s_k] \geq 0$. The last term on the rhs of Eq. (70) is the "pinning force," responsible for *phase-locking*. Like in the Kuramoto model, there exists a threshold above which *synchronization* occurs. This synchronization threshold is here given by

$$\gamma_k \geq |\omega_k - \omega_{\mathrm{res}}|. \quad (71)$$

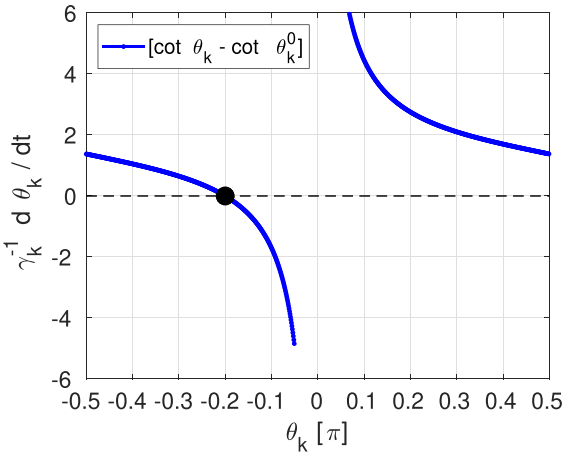

FIG. 6. Phase response curve $\frac{d\theta_k}{dt} = f(\theta_k)$ for the CTEM fluid model. The curve is shown for a value $\theta_k^0 = -0.2\pi$ of the phase-locked solution.

In most regimes, however, the timescale of the crossphase dynamics is so short that the crossphase directly locks to its linear value, without a transient. However, near marginality, the crossphase is expected to exhibit a slow dynamics. In analogy with the "phase response curve" associated with oscillators with global couplings, one can define the "crossphase response" curve (CPR) as the rhs of Eq. (70). The crossphase response curve is plotted for a value $\theta_k^0 = 0.2\pi$ (Fig. 6). A similar idea was introduced in Refs. 13 and 36.

Remember that θ_k is the *instantaneous* crossphase between n_{ik} and ϕ_k. Equation (70) can be further linearized around the phase-locked crossphase (34). Using the Taylor series $\cot\theta_k \simeq \cot\theta_k^0 + \cot'(\theta_k^0)[\theta_k - \theta_k^0]$, one obtains, after some algebra

$$\frac{\partial\theta_k}{\partial t} \simeq -\frac{1}{\tau_k}(\theta_k - \theta_k^0), \tag{72}$$

where τ_k is the linear response time (relaxation time) at wavenumber $\mathbf{k}$

$$\tau_k = \left[(1+\cot^2\theta_k^0)\gamma_k\right]^{-1}, \tag{73}$$

which is of the order of the turbulence correlation time τ_c, i.e., $\tau_k \propto {\gamma_k}^{-1} \sim \tau_c$, when taking into account resonance-broadening due to turbulence, i.e., $\gamma_k \to \gamma_k + D_t k_\perp^2$, with D_t the turbulent diffusivity. Note that the crossphase dynamics—for particle transport—Eq. (72) has a similar form as the heat flux dynamics of the traffic-jam model of Refs. 37 and 38

$$\frac{\partial Q}{\partial t} = -\frac{1}{\tau}(Q - Q_0), \tag{74}$$

where $Q = \sum_k Q_k$ is the heat flux, $Q_0 = \sum_k Q_k^0$ is the mean heat flux, and τ is the response time between the instantaneous heat-flux and its relaxed value, which is also of the order of the turbulence correlation time.[37,39] From the crossphase dynamics Eq. (72), one sees that the relaxation time becomes very large $\tau_k \to \infty$, when the system is near marginality $\gamma_k \to 0$. Hence, one expects a *slow dynamics* of the crossphase (and associated particle flux) close to marginality, where the crossphase can remain far from their phase-locked value (the crossphase usually assumed in quasi-linear transport codes), for a significant time. Hence, there seems to be a connection between the "traffic-jam" model of Refs. 37 and 38 for heat transport, and the CTEM crossphase dynamics for particle transport. More work needs to be done to better understand this connection. At this point, one may ask: Why bother with studying the linear crossphase dynamics, since nonlinear mode-coupling effects will certainly be important? Note, however, that for weak-turbulence (valid near marginality), nonlinear effects are usually quadratic and involve disparate-scale interactions. In other words, they correspond to a modification of flows (zonal flows) and profiles (zonal density, zonal T_e, …). We thus believe that the linear crossphase dynamics (which contains diamagnetic frequency terms, and hence profile gradients) is a good starting point for the extension to weak turbulence.

The crossphase between electron temperature fluctuations T_{ek} and potential fluctuations ϕ_k is defined as

$$\chi_k = \arg\left(\frac{\phi_k}{T_{ek}}\right) = \arg\left(\frac{\phi_k}{s_{ek}}\right). \tag{75}$$

It is straightforward to show that the dynamics of the crossphase χ_k takes the form

$$\frac{\partial\chi_k}{\partial t} = \omega_{\rm res} - \omega_k + \left(\eta_e - \frac{2}{3}\right)\omega_* \beta_k^e \cos\chi_k + \frac{10}{9 f_t}\omega_{de}\frac{\beta_k^e}{\alpha_k^e}\cos(\chi_k - \theta_k^0), \tag{76}$$

where $\omega_{\rm res} = \frac{5}{3}\omega_{de}$ is the trapped-electron resonance frequency, and $\alpha_k^e = |\phi_k|/|n_k|$, $\beta_k^e = |\phi_k|/|s_{ek}|$ are the amplitude ratios for electrons, given by

$$\alpha_k^e = \frac{1 + \frac{10}{9}(\omega_{de}^2/{\gamma_k}^2)\sin^2(\chi_k - \theta_k^0)}{f_t[(\omega_* - \omega_{de})/\gamma_k]\sin\theta_k^0 + f_t\left(\eta_e - \frac{2}{3}\right)(\omega_*\omega_{de}/{\gamma_k}^2)\sin\chi_k\sin(\chi_k - \theta_k^0)}, \tag{77}$$

$$\beta_k^e = \frac{1 + \frac{10}{9}(\omega_{de}^2/{\gamma_k}^2)\sin^2(\chi_k - \theta_k^0)}{\left(\eta_e - \frac{2}{3}\right)(\omega_*/\gamma_k)\sin\chi_k + \frac{10}{9}\left[(\omega_* - \omega_{de})\omega_{de}/{\gamma_k}^2\right]\sin\theta_k^0\sin(\chi_k - \theta_k^0)}. \tag{78}$$

Since the dynamics of the θ_k crossphase is set by the ions only, Eq. (33), this crossphase was set to its phase-locked value $\theta_k \simeq \theta_k^0$, expression (34).

Note that, for the CTEM model, the turbulent particle flux and electron heat flux can be written in the form

$$\Gamma = \sum_k k_y \frac{|\phi_k|^2}{\alpha_k} \sin\theta_k, \quad \text{and} \quad Q_e = \sum_k k_y \frac{|\phi_k|^2}{\beta_k^e} \sin\chi_k, \tag{79}$$

where α_k is given by expression (32). Replacing the amplitude ratio α_k by its expression (32), Γ can be further simplified

$$\Gamma = \sum_k k_y \frac{\omega_* + \tau\omega_{di}}{\gamma_k} |\phi_k|^2 \sin^2\theta_k. \tag{80}$$

IV. DISCUSSION AND CONCLUSIONS

Let us first discuss the comparison of the fluid model and the linear gyrokinetic simulations using the GKPSP code.[15] In the ITG case, the fluid model (42) and (43) only shows qualitative similarity with the gyrokinetic simulation. However, the ITG frequency is more closely matched to the gyrokinetic result than the growth rate, which shows a large difference. Frequency and growth rate were also compared with Nilsson *et al.*[8] The ITG frequency from the ITG model used in this work[29] more closely matches the gyrokinetic result compared to that of Ref. 8, except for $k_y\rho_s \ll 1$. For the CTEM case also, only qualitative similarity is found between the fluid model and GKPSP simulation, except at low wavenumbers $k_y\rho_s < 0.2$. Let us now discuss the Kuramoto-like equation (70) describing the dynamics of the crossphase between density and potential fluctuations of the fluid CTEM model. Equation (70) is very similar to the Kuramoto equation,[35] except that the associated phase-response curve is of the form "cotangent" instead of a sinusoid for the Kuramoto model. It thus has period π instead of 2π for the Kuramoto model. One particular interesting property of the Kuramoto model is the synchronization of coupled oscillators if the coupling is above a certain threshold K_{th} proportional to the entrainment frequency. By analogy, we may say, that for CTEM, the transport *crossphase*—associated with particle transport—at different wave-numbers become synchronized when above the threshold. For CTEM, the threshold depends on the difference between the mode frequency and the *resonance* frequency. The form of the Kuramoto-like equation (70) for the CTEM instability, which is a reactive instability is very different than the one for the collisional drift-wave instability or the weakly dissipative trapped electron mode (DTEM).[13] In the latter case, the cotangent function on the rhs of Eq. (70) is replaced by the (negative of the) tangent function, and it is multiplied by the electron–ion collision frequency ν_{ei} instead of the linear growth rate, since $\gamma_k \ll \nu_{ei}$ for collisional instabilities. This may partly explain the difference between the nature of the two types of instabilities.

In future work, the nonlinear dynamics of the CTEM model will be investigated, especially the zonal flows and associated zonal density and zonal T_e corrugations and their impact on particle transport, electron heat transport, and staircase formation.[16–18,37] For these future studies, one obvious limitation of our model is the assumption of passing adiabatic electrons.

ACKNOWLEDGMENTS

The authors would like to thank Jae-Min Kwon, Sumin Yi, Sehoon Ko, P. H. Diamond, I. Dodin, and X. Garbet for helpful discussions. This work was supported by R&D Program through Korean Institute of Fusion Energy (KFE) funded by the Ministry of Science and ICT of the Republic of Korea (No. KFE-EN2441-10).

AUTHOR DECLARATIONS

Conflict of Interest

The authors have no conflicts to disclose.

Author Contributions

Michael Leconte: Conceptualization (equal); Data curation (equal); Writing – review & editing (equal). **Lei Qi:** Conceptualization (equal); Data curation (equal); Writing – review & editing (equal). **Johan Anderson:** Conceptualization (equal); Data curation (equal); Writing – review & editing (equal).

DATA AVAILABILITY

The data that support the findings of this study are available from the corresponding author upon reasonable request.

APPENDIX A: CTEM LIMIT OF THE CHALMERS MODEL

Linearizing the original system (1)–(4) for $g_i = g_e = 1$, one obtains

$$-i\omega n_k + if_t\omega_*\phi_k = -i\omega_{de}(n_k - f_t\phi_k + f_t T_{ek}), \tag{A1}$$

$$-i\omega T_{ek} + i\eta_e\omega_*\phi_k = -\frac{2}{3f_t} i\omega_{de}\left(n_k - f_t\phi_k + \frac{7}{2} f_t T_{ek}\right), \tag{A2}$$

$$\begin{aligned} &-(1-f_t+k_\perp^2)i\omega\phi_k + i\left(1 - f_t - \frac{1+\eta_i}{\tau}k_\perp^2\right)\omega_*\phi_k \\ &= i\omega_{de}[(1-f_t)(1+1/\tau)\phi_k + T_{ik} + (1+1/\tau)n_k + f_t T_{ek}], \end{aligned} \tag{A3}$$

$$\begin{aligned} -i\omega T_{ik} = {} & i\frac{\omega_{de}}{\tau}\left[\frac{2}{3\tau}(1-f_t+\tau)\phi_k + \frac{2}{3\tau}n_k + \frac{7}{3}T_{ik}\right] \\ & - i\left[\eta_i - \frac{2}{3\tau}(1+\eta_i+\tau)k_\perp^2\right]\frac{\omega_*}{\tau}\phi_k \\ & - \frac{2}{3\tau^2} ik_\perp^2\omega_{de}\left[(1+\tau)\phi_k + \frac{\tau}{1-f_t}T_{ik} + \frac{1+\tau}{1-f_t}n_k + \frac{\tau f_t}{1-f_t}T_{ek}\right], \end{aligned} \tag{A4}$$

with $\omega_* = k_y v_{*e}$ the electron diamagnetic frequency, and $\omega_{de} = \epsilon_n\omega_*$ the precession-drift frequency. The linear dispersion relation is best obtained by first transforming the system. Adding Eqs. (A1) and (A3) yields the ion continuity equation

$$\begin{aligned} &-i\omega(n_{ik} + k_\perp^2\phi_k) + \left(1 - \frac{1+\eta_i}{\tau}k_\perp^2\right)i\omega_*\phi_k \\ &= i\frac{\omega_{de}}{\tau}[(1-f_t+\tau)\phi_k + n_k + \tau T_{ik}] \end{aligned} \tag{A5}$$

with, due to quasi-neutrality, $n_{ik} = n_k + (1-f_t)\phi_k$ the ion density perturbation. This can also be written as

$$\begin{aligned} &-i\omega(n_{ik} + k_\perp^2\phi_k) + \left(1 - \frac{1+\eta_i}{\tau}k_\perp^2\right)i\omega_*\phi_k \\ &= -i\omega_{di}(\tau\phi_k + n_{ik} + \tau T_{ik}) \end{aligned} \tag{A6}$$

with $\omega_{di} = -\omega_{de}/\tau < 0$ the ion magnetic drift. Introducing the gyrocenter ion density $n_{ik}^{GC} = n_{ik} + k_\perp^2 \phi_k$, one obtains

$$-i\omega n_{ik}^{GC} + \left(1 - \frac{1+\eta_i}{\tau} k_\perp^2\right) i\omega_* \phi_k = -i\omega_{di}(\tau\phi_k + n_{ik}^{GC} - k_\perp^2 \phi_k + \tau T_{ik}). \tag{A7}$$

The gyrocenter ion density response is then

$$(\omega - \omega_{di}) n_{ik}^{GC} = \left[\omega_* + (\tau - k_\perp^2)\omega_{di} - k_\perp^2(\omega + \alpha_i\omega_*)\right]\phi_k + \tau\omega_{di} T_{ik}, \tag{A8}$$

where $\alpha_i = (1+\eta_i)/\tau$ represents ion FLR effects. Multiplying Eq. (A4) by 3/2 and subtracting Eq. (A7) yields the ion heat balance

$$-i\omega\left[\frac{3}{2} T_{ik} - \frac{1-f_t}{\tau}\phi_k - \frac{n_k}{\tau}\right] - \frac{3}{2} i\left(\eta_i - \frac{2}{3}\right)\frac{\omega_*}{\tau}\phi_k = -\frac{5}{2} i\omega_{di} T_{ik}. \tag{A9}$$

The associated linear ion temperature response is

$$T_{ik} = \frac{1}{\omega - \frac{5}{3}\omega_{di}}\left[\left(\eta_i - \frac{2}{3}\right)\frac{\omega_*}{\tau}\phi_k + \frac{2}{3\tau}\omega(n_{ik}^{GC} - k_\perp^2\phi_k)\right]. \tag{A10}$$

Replacing T_{ik} in terms of n_{ik}^{GC} and ϕ_k in Eq. (A8), the gyrocenter ion density response takes the form

$$n_{ik}^{GC} - k_\perp^2\phi_k = \frac{(\omega_* + \tau\omega_{di})\left(\omega - \frac{5}{3}\omega_{di}\right) - k_\perp^2(\omega + \alpha_i\omega_*)\left(\omega - \frac{5}{3}\omega_{di}\right) + \left(\eta_i - \frac{2}{3}\right)\omega_*\omega_{di}}{N_i}\phi_k \tag{A11}$$

with $N_i = \omega^2 - \frac{10}{3}\omega_{di}\omega + \frac{5}{3}\omega_{di}^2$. Next, we analyze the linear electron dynamics. Multiplying Eq. (A2) by $\frac{3}{2} f_t$ and subtracting Eq. (A1), one obtains the electron heat balance

$$-i\omega\left[\frac{3}{2} f_t T_{ek} - n_k\right] + \frac{3}{2} i f_t\left[\eta_e - \frac{2}{3}\right]\omega_*\phi_k = -\frac{5}{2} i f_t \omega_{de} T_{ek}. \tag{A12}$$

This yields the linear electron temperature response

$$T_{ek} = \frac{1}{f_t\left(\omega - \frac{5}{3}\omega_{de}\right)}\left[\left(\eta_e - \frac{2}{3}\right) f_t\omega_*\phi_k + \frac{2}{3}\omega n_k\right]. \tag{A13}$$

Expressing T_{ek} in terms of ϕ_k and n_k, the linear electron density response is then

$$(\omega - \omega_{de}) n_k = f_t(\omega_* - \omega_{de})\phi_k + \frac{\omega_{de}}{\omega - \frac{5}{3}\omega_{de}}\left[\frac{2}{3}\omega n_k + f_t\omega_*\left(\eta_e - \frac{2}{3}\right)\phi_k\right]. \tag{A14}$$

After some algebra, one obtains

$$n_k = f_t\left[\omega - \omega_{de} - \frac{2}{3}\frac{\omega_{de}\omega}{\omega - \frac{5}{3}\omega_{de}}\right]^{-1}\left[\omega_* - \omega_{de} + \left(\eta_e - \frac{2}{3}\right)\frac{\omega_*\omega_{de}}{\omega - \frac{5}{3}\omega_{de}}\right]\phi_k. \tag{A15}$$

Note the identity $\omega_{de}\left(1 + \frac{5}{3}\delta\right) = \omega\delta$, with $\delta = \omega_{de}/\left(\omega - \frac{5}{3}\omega_{de}\right)$ obtained in Ref. 40. The denominator can be rewritten as $\omega - \frac{5}{3}\omega_{de}\left(1 + \frac{2}{3}\delta\right) = \omega - \frac{5}{3}(\omega - \omega_{de})\delta$. Then, multiplying both numerator and denominator of expression (A15) by $\omega - \frac{5}{3}\omega_{de}$, one obtains—after some algebra—the following linear trapped-electron density response:

$$n_k = f_t\frac{(\omega_* - \omega_{de})\left(\omega - \frac{5}{3}\omega_{de}\right) + \left(\eta_e - \frac{2}{3}\right)\omega_*\omega_{de}}{N_e}\phi_k, \tag{A16}$$

with $N_e = \omega^2 - \frac{10}{3}\omega_{de}\omega + \frac{5}{3}\omega_{de}^2$. Finally, using quasi-neutrality in the form $(1 - f_t + k_\perp^2)\phi_k = n_{ik}^{GC} - n_k$ yields the following linear dispersion relation:

$$\frac{n_{i,k}^{GC} - k_\perp^2\phi_k}{\phi_k} = f_t\frac{(\omega_* - \omega_{de})\left(\omega - \frac{5}{3}\omega_{de}\right) + \left(\eta_e - \frac{2}{3}\right)\omega_*\omega_{de}}{N_e} + 1 - f_t. \tag{A17}$$

In the limit of CTEM, the mode frequency resonates with the precession-drift frequency $\omega \sim \frac{5}{3}\omega_{de}$. In this limit, $N_i \gg N_e$, i.e., the ion diamagnetic resonance is not important $\omega_k - \omega_{di} \sim \omega_k$, ion temperature fluctuations are negligible $|T_{ik}| \ll 1$, and the dispersion relation (A17) reduces to

$$1 - f_t + k_\perp^2 - \frac{(1 - k_\perp^2/\tau)\omega_* + \tau\omega_{di}}{\omega} + f_t\frac{(\omega_* - \omega_{de})\left(\omega - \frac{5}{3}\omega_{de}\right) + \left(\eta_e - \frac{2}{3}\right)\omega_*\omega_{de}}{N_e} \simeq 0. \tag{A18}$$

APPENDIX B: SOLVING THE CTEM CUBIC DISPERSION RELATION

To decrease the number of free parameters, the CTEM cubic dispersion relation (A18) is solved at fixed $f_t = 1/2$ and $\tau = 1$. The CTEM cubic dispersion relation to solve is

$$(1 + 2k_\perp^2)\omega^3 - \left[(1 + 2k_\perp^2)\frac{10}{3}\omega_{de} - (\omega_* - \omega_{de}) + 2\left((1 - k_\perp^2)\omega_* - \omega_{de}\right)\right]\omega^2 + \left[\left(\eta_e - \frac{2}{3}\right)\omega_*\omega_{de} + (1 + 2k_\perp^2)\frac{5}{3}\omega_{de}^2 - \frac{5}{3}\omega_{de}(\omega_* - \omega_{de}) + \frac{20}{3}\omega_{de}\left((1 - k_\perp^2)\omega_* - \omega_{de}\right)\right]\omega - \frac{10}{3}\omega_{de}^2\left[(1 - k_\perp^2)\omega_* - \omega_{de}\right] = 0. \tag{B1}$$

This dispersion relation is in normalized form

$$A\omega^3 + B\omega^2 + C\omega + D = 0 \tag{B2}$$

with real-valued coefficients

$$A = 1 + 2k_\perp^2,$$
$$B = -\left[(1+2k_\perp^2)\frac{10}{3}\epsilon_n - (1-\epsilon_n) + 2(1-\epsilon_n-k_\perp^2)\right],$$
$$C = \left(\eta_e - \frac{2}{3}\right)\epsilon_n + (1+2k_\perp^2)\frac{5}{3}\epsilon_n^2 - \frac{5}{3}\epsilon_n(1-\epsilon_n) + \frac{20}{3}\epsilon_n(1-\epsilon_n-k_\perp^2).$$
$$D = -\frac{10}{3}\epsilon_n^2(1-\epsilon_n-k_\perp^2).$$

The solution can be obtained by first "depressing" the cubic—transforming to a form without quadratic term—and then using the cubic formula. Using the change of variables

$$p = \frac{1}{A}\left[C - 3A(\omega_{k0})^2\right], \tag{B3}$$

$$q = \frac{2B^3 - 9ABC + 27A^2D}{27A^3} \tag{B4}$$

$$= AC\omega_{k0} - 2(\omega_{k0})^3 + \frac{D}{A} \tag{B5}$$

with

$$\omega_{k0} = -\frac{B}{3A}. \tag{B6}$$

Note that $\omega_{k0} \geq 0$, i.e., in the electron diamagnetic direction. In our case,

$$\omega_{k0} = \frac{k_y}{3(1+2k_\perp^2)}\left[(1+2k_\perp^2)\frac{10}{3}\epsilon_n - (1-\epsilon_n) + 2(1-\epsilon_n-k_\perp^2)\right]. \tag{B7}$$

The cubic equation (B2) reduces to the depressed cubic equation

$$\hat{\omega}^3 + p\hat{\omega} + q = 0, \tag{B8}$$

where $\hat{\omega} = \omega - \omega_{k0}$.

We may now use Cardano's "cubic formula" in the special case of $s = s_k, t = t_k$ real-valued

$$\hat{\omega}_{k0} = \Omega_0 s_k + \Omega_0^* t_k, \tag{B9}$$
$$\hat{\omega}_{k1} = \Omega_1 s_k + \Omega_1^* t_k, \tag{B10}$$
$$\hat{\omega}_{k2} = \Omega_2 s_k + \Omega_2^* t_k \tag{B11}$$

with the real parameters s, t, and complex parameters $\Omega_0, \Omega_1, \Omega_2$ given, respectively, by

$$s_k = \left[-\frac{q}{2} + \sqrt{\frac{q^2}{4} + \frac{p^3}{27}}\right]^{1/3}, \tag{B12}$$

$$t_k = \left[-\frac{q}{2} - \sqrt{\frac{q^2}{4} + \frac{p^3}{27}}\right]^{1/3}, \tag{B13}$$

$$\Omega_l = e^{2il\pi/3}, \quad l = 0, 1, 2. \tag{B14}$$

Here, the quantities Ω_l are the cubic roots of 1. More specifically,

$$\Omega_0 = 1, \quad \Omega_1 = e^{2i\pi/3}, \quad \Omega_2 = \Omega_1^* = e^{-2i\pi/3}. \tag{B15}$$

Physically, there is one marginally stable mode with real frequency $\omega_k = \omega_{k0} + s + t$ (a remnant of the ITG branch, due to ion density response) and two complex-conjugate modes $\omega_k^{\pm} = \omega_{k0} + e^{\pm 2i\pi/3}s + e^{\mp 2i\pi/3}t$. Let us now write down explicitly the parameters of the depressed cubic. The parameter p is given by

$$p = \frac{k_y}{1+2k_\perp^2}\left[\left(\eta_e - \frac{2}{3}\right)\epsilon_n + (1+2k_\perp^2)\frac{5}{3}\epsilon_n^2 - \frac{5}{3}\epsilon_n(1-\epsilon_n) + \frac{20}{3}\epsilon_n(1-\epsilon_n-k_\perp^2) - 3(1+2k_\perp^2)(\omega_{k0})^2\right], \tag{B16}$$

with ω_{k0} given by expression (B7). The parameter q takes the form

$$q = k_y^2(1+2k_\perp^2)\omega_{k0}\left[\left(\eta_e - \frac{2}{3}\right)\epsilon_n + (1+2k_\perp^2)\frac{5}{3}\epsilon_n^2 - \frac{5}{3}\epsilon_n(1-\epsilon_n) + \frac{20}{3}\epsilon_n(1-\epsilon_n-k_\perp^2)\right] - 2(\omega_{k0})^3 - \frac{1}{1+2k_\perp^2}\left[\frac{10}{3}\epsilon_n^2(1-\epsilon_n-k_\perp^2)\right]. \tag{B17}$$

Hence, above threshold $\eta_e \geq \eta_e^c$ (to be determined *a posteriori*), one expects

$$q \geq 0. \tag{B18}$$

Similarly, one also expects

$$p \geq 0. \tag{B19}$$

Hence, this implies

$$t_k \leq 0. \tag{B20}$$

Moreover, since $q \geq 0$, this directly implies the following inequality: $|t_k| \geq s_k$, while the quantity s_k can be positive or negative, depending on the sign of the quantity $\Delta_3 = -q/2 + \sqrt{q^2/4 + p^3/27}$ inside the cube-root in expression (B12). If $\Delta_3 \geq 0$, then $s_k \geq 0$, while if $\Delta_3 \leq 0$, then $s_k \leq 0$. However, it is easy to see that since $p \geq 0$, this implies $p^3 \geq 0$ and hence $\Delta_3 \geq 0$ and $s_k \geq 0$. Therefore, one has: $s_k \geq 0$, and $t_k \leq 0$.

Physically, the modes real and complex-values frequencies formally take the form

$$\omega_k{}^0 = \omega_{k0} - [|t_k| - s_k], \quad \gamma_k{}^0 = 0, \tag{B21}$$

$$\omega_k{}^+ = \omega_{k0} + \cos\left(\frac{\pi}{3}\right)[|t_k| - s_k], \quad \gamma_k{}^+ = \sin\left(\frac{\pi}{3}\right)[|t_k| - s_k], \tag{B22}$$

$$\omega_k{}^- = \omega_{k0} + \cos\left(\frac{\pi}{3}\right)[|t_k| - s_k] \quad \gamma_k{}^- = -\sin\left(\frac{\pi}{3}\right)[|t_k| - s_k] \tag{B23}$$

with $\omega = \omega_k + i\gamma_k$ the complex-valued frequency. Here, we used the trigonometric identities: $\cos 2\pi/3 = -\cos \pi/3$ and $\sin(2\pi/3) = \sin(\pi/3)$, to move the angle to the first quadrant.

REFERENCES

[1]C. Bourdelle, X. Garbet, F. Imbeaux, A. Casati, N. Dubuit, R. Guirlet, and T. Parisot, Phys. Plasmas **14**, 112501 (2007).
[2]C. Angioni, E. Fable, M. Greenwald, M. Maslov, A. G. Peeters, H. Takenaga, and H. Weisen, Plasma Phys. Controlled Fusion **51**, 124017 (2009).
[3]C. Angioni, Y. Camenen, F. J. Casson, E. Fable, R. M. McDermott, A. G. Peeters, and J. E. Rice, Nucl. Fusion **52**, 114003 (2012).
[4]J. C. Adam, W. M. Tang, and P. H. Rutherford, Phys. Fluids **19**, 561 (1976).
[5]J. Weiland, *Collective Modes in Inhomogeneous Plasmas, Kinetic and Advanced Fluid Theory* (IOP Publishing, Bristol, 2000), p. 115.
[6]J. Weiland, A. B. Jarmen, and H. Nordman, Nucl. Fusion **29**, 1810 (1989).
[7]H. Nordman, J. Weiland, and A. Jarmen, Nucl. Fusion **30**, 983 (1990).
[8]J. Nilsson, M. Liljestrom, and J. Weiland, Phys. Fluids B **2**, 2568 (1990).
[9]A. Jarmen, P. Anderson, and J. Weiland, Nucl. Fusion **27**, 941 (1987).
[10]J. Anderson, H. Nordman, R. Singh, and J. Weiland, Plasma Phys. Controlled Fusion **48**, 651 (2006).
[11]M. Leconte and T. Kobayashi, Phys. Plasmas **28**, 014503 (2021).
[12]M. Sasaki, K. Itoh, B. F. McMillan, T. Kobayashi, H. Arakawa, and J. Chowdhury, Phys. Plasmas **28**, 112304 (2021).
[13]M. Leconte and R. Singh, Plasma Phys. Controlled Fusion **61**, 095004 (2019).
[14]C. Y. An, B. Min, and C. B. Kim, Plasma Phys. Controlled Fusion **59**, 115006 (2017).
[15]J. M. Kwon, L. Qi, S. Yi, and T. S. Hahm, Comput. Phys. Commun. **215**, 81 (2017).
[16]G. Dif-Pradalier, G. Hornung, P. Ghendrih, Y. Sarazin, F. Clairet, L. Vermare, P. H. Diamond, J. Abiteboul, T. Cartier-Michaud, C. Ehrlacher *et al.*, Phys. Rev. Lett. **114**, 085004 (2015).
[17]G. Dif-Pradalier, G. Hornung, X. Garbet, P. Ghendrih, V. Grandgirard, G. Latu, and Y. Sarazin, Nucl. Fusion **57**, 066026 (2017).
[18]L. Qi, M. J. Choi, M. Leconte, T. S. Hahm, and J. M. Kwon, Nucl. Fusion **62**, 126025 (2022).
[19]X. Garbet, O. Panico, R. Varennes, C. Gillot, G. Dif-Pradalier, Y. Sarazin, V. Grandgirard, P. Ghendrih, and L. Vermare, Phys. Plasmas **28**, 042302 (2021).
[20]E. Fable, C. Angioni, and O. Sauter, Plasma. Phys. Controlled Fusion **52**, 015007 (2010).
[21]A. I. Dyachenko, S. V. Nazarenko, and V. E. Zakharov, Phys. Lett. A **165**, 330 (1992).
[22]M. A. Malkov, P. H. Diamond, and M. N. Rosenbluth, Phys. Plasmas **8**, 5073 (2001).
[23]J. Y. Lang, S. E. Parker, and Y. Chen, Phys. Plasmas **15**, 055907 (2008).
[24]T. S. Hahm and W. M. Tang, Phys. Plasmas **3**, 242 (1996).
[25]J. Anderson and H. Nordman, J. Plasma Phys. **72**(5), 609 (2006).
[26]X. Garbet, L. Garzotti, P. Mantica, H. Nordman, M. Valovic, H. Weisen, and C. Angioni, Phys. Rev. Lett. **91**, 035001 (2003).
[27]P. H. Diamond, see https://courses.physics.ucsd.edu/2021/Spring/physics218c/lecture.html for "Lectures from UC San Diego Physics 218C, Spring" (2021).
[28]X. Garbet, N. Dubuit, E. Asp, Y. Sarazin, C. Bourdelle, P. Ghendrih, and G. T. Hoang, Phys. Plasmas **12**, 082511 (2005).
[29]J. Anderson, H. Nordman, R. Singh, and J. Weiland, Phys. Plasmas **9**, 4500 (2002).
[30]H. Nordman, B. Jhowry, and J. Weiland, Phys. Fluids B **05**, 3465 (1993).
[31]M. A. Beer, "Gyrofluid models of turbulent transport in tokamaks," Ph.D. thesis (Princeton University, 1995).
[32]R. Singh and P. H. Diamond, Plasma Phys. Controlled Fusion **63**, 035015 (2021).
[33]A. I. Smolyakov, P. H. Diamond, and M. V. Medvedev, Phys. Plasmas **7**, 3987 (2000).
[34]Y. Zhou, H. Zhu, and I. Dodin, Plasma Phys. Controlled Fusion **61**, 075003 (2019).
[35]J. A. Acebron, L. L. Bonilla, J. C. Perez Vicente, F. Ritort, and R. Spigler, Rev. Mod. Phys. **77**, 137 (2005).
[36]Z. B. Guo and P. H. Diamond, Phys. Rev. Lett. **114**, 145002 (2015).
[37]Y. Kosuga, P. H. Diamond, G. Dif-Pradalier, and O. D. Gurcan, Phys. Plasmas **21**, 055701 (2014).
[38]O. D. Gurcan, P. H. Diamond, X. Garbet, V. Berionni, G. Dif-Pradalier, P. Hennequin, P. Morel, Y. Kosuga, and L. Vermare, Phys. Plasmas **20**, 022307 (2013).
[39]L. Qi, J. M. Kwon, T. S. Hahm, S. Yi, and M. J. Choi, Nucl. Fusion **59**, 026013 (2019).
[40]A. Jarmen and H. Nordman, Plasma Phys. Controlled Fusion **34**, 749 (1992).